Cite as: Manzanal, D., Bertelli, S., Lopez-Querol, S. *et al.* Influence of fines content on liquefaction from a critical state framework: the Christchurch earthquake case study. *Bull Eng Geol Environ* **80**, 4871–4889 (2021). https://doi.org/10.1007/s10064-021-02217-2

Influence of Fines Content on Liquefaction from a Critical State Framework: the Christchurch Earthquake Case Study

Diego Manzanal[1], Silvia Bertelli[2,3], Susana Lopez-Querol[2,4], Tiziana Rossetto[2,5] and Pablo Mira[6]

1 Technical University of Madrid; d.manzanal@upm.es

2 University College London, Department of Civil, Environmental and Geomatic Engineering

3 silvia.bertelli@ucl.ac.uk

4 s.lopez-querol@ucl.ac.uk

5 t.rossetto@ucl.ac.uk

6 Laboratorio de Geotecnia CEDEX (Madrid); pablo.mira@cedex.es

ABSTRACT: In earthquake engineering practice, the liquefaction potential of soils is commonly evaluated through simplified procedures. These approaches are suitable for sands with very low to no fines content, which have been traditionally thought to be the only liquefiable materials. However, field observations and experimental research have extensively demonstrated that low plasticity silty sands can also be highly liquefiable. Thus, this paper investigates the effect of non-plastic fines contents on the liquefaction potential of soils, taking the 2010-2011 Canterbury Earthquake Sequence as a case study. The validity of standard simplified procedures for high fines content soils is critically evaluated and compared with a finite element model based on a full solid-fluid coupled formulation. The model includes a

state parameter-based constitutive law within the Generalised Plasticity theory, which allows the fines content to be taken into account explicitly. The standard simplified procedures are shown to be less effective in the evaluation of liquefaction potential in soils with high fines content but are still indispensable tools for evaluating the performance of soils over large urban areas. As the main conclusion, it is recommended that empirical models are complemented with an advanced numerical analysis in those cases where silty sands with high fines content are identified, as its outcomes can more realistically represent the soil behaviour during a seismic event.

KEYWORDS: Liquefaction potential, Generalized Plasticity, Critical state framework, Silty sands, low-plasticity fines, Canterbury Earthquake Sequence

1. INTRODUCTION

Liquefaction resistance of sands with fines is commonly evaluated using simplified approaches that are based on research conducted on clean sands. The first simplified liquefaction assessment procedure was developed in the early 1970s based on the Standard Penetration Test (SPT) (Seed and Idriss, 1971). Since then, several other such procedures have been proposed that use different types of in-situ tests as input. The simplified approach has been established as state-of-practice liquefaction assessment procedure due to its simplicity and limited required computational effort (Youd and Idriss, 2001; Kayabasi and Gokceoglu, 2018). However, simplified liquefaction evaluation relationships have proven to have low accuracy when applied to silty sands (Ecemis and Karaman, 2014) as they do not quantify the influence of both the structure and fabric of the soil appropriately (Taylor, 2015).

The role of Fines Content (FC) on liquefaction susceptibility has been extensively studied through experimental research. Some authors indicate that FC increases the resistance to liquefaction (Pitman et al., 1994), and thus mainly clean sand with low FC content is susceptible to liquefaction. For instance, the SPT-based and CPT-based simplified approach relationships shift to the left as the FC increases (Idriss, 1999, Youd and Idriss, 2001; Idriss and Boulanger, 2004, 2008; Boulanger and Idriss, 2014), which result in higher soil resistance to liquefaction. However, other authors find that the increase FC makes the soil more susceptible to liquefaction (Lade et al., 1994). More recent studies on the grain size and composition of sand blows ejected in representative sites affected by the 2012 Emilia-Romagna Earthquake show that silty sands and silts are characterized by a relatively high FC can liquefy (Fontana et al., 2019; Amoroso et al., 2020). Cavallaro et al. (2018) present an alternative approach to analysing the liquefaction phenomena produced during Emilia-Romagna Earthquake with Seismic Dilatometer Marchetti Tests (SDMT). Generally, sand behaviour has

a strong dependence on voids ratio and effective stress (Been and Jefferies, 1985; Ishihara, 1993; Hird and Hassona, 1990; Jiang et al., 2015). This means that neither voids ratio nor effective stress alone can fully characterise sand behaviour, and both need to be taken into account.

The critical state framework comes into play to encompass the effects of void ratio and effective stress on soil performance. When soil is subjected to failure, it reaches its critical state, defined by the volume (under drained conditions) or confined stress p' (for undrained situations). The soil tends towards a critical state, independently from its initial conditions. Instead, the state parameter indicates how far the current state of soil is from its critical state, usually in terms of unitary volume (or void ratio e), (Been and Jefferies, 1985).

The Critical State Line (CSL) separates the initial states of the soil into contractive and dilative regions in the $e - p'$ plane (Been and Jefferies, 1985; Ishihara, 1993). Experimental evidence demonstrates that the CSL moves vertically and rotates anticlockwise when the FC increases from 0 to 30% (Zlatović and Ishihara, 1995). This effect has also been observed in sandy soils in cases where their grains break during shearing (Bandini and Coop, 2011). The definition of the CSL for silty sands depends on the FC. The contractive or dilative behaviour of these soils depends on the relative position of its initial state defined by the state parameter. The location of the CSL and initial state parameter of soil has proven to be affected on its response under dynamic loads, governing its liquefaction response (Qadimi and Coop, 2007; López-Querol and Coop, 2012). Thus, in any critical state-based constitutive model, the liquefaction resistance can be evaluated if the location of the CSL is adequately defined.

Soil behaviour during an earthquake is a complex phenomenon that can be comprehensively analysed through numerical simulations. Nonetheless, the ability of these numerical simulations to reproduce the soil behaviour during cyclic loading depends, among other factors,

on the adopted constitutive soil model. For instance, the Generalised Plasticity state parameter-based model, proposed by Manzanal *et al.*(2011a; 2011b; 2010), (referred to as MPZ hereinafter), is suitable to reproduce phenomena such as liquefaction under monotonic loading and complex phenomena observed during cyclic loadings as well, such as cyclic mobility and densification. The constitutive behaviour of sands with non-plastic fines has been studied throughout the concept of equivalent void ratio e* (Thevanayagam, 1998; Yang et al., 2006; Rahman et al., 2014) or assuming equivalent steady-state lines (Rahman et al., 2008) or reference state curve (Javanmardi et al. 2017). All these approaches are based on laboratory mixtures of sand with non-plastic fines. For natural soils from clean sand to silty sand, the state parameter ψ has been proved to capture different soil behaviour in a unified manner regardless of soil type or FC (Jefferies and Been, 2016). State-dependent MPZ constitutive model can capture changes in the CSL location for soils with different FC, which makes it a unique tool to explore the soil performance during an earthquake when the FC might play a significant role.

During the 2010-2011 Canterbury Earthquake Sequence (CES), severe and extensive liquefaction manifestations associated with natural sands and silty sand deposits were observed (Taylor, 2015). After this sequence, significant site investigations and laboratory analyses were performed and made publically available through the New Zealand Geotechnical Database (NZGD), (Ministry for Business Innovation & Employment, 2018). These show that in many locations where liquefaction manifestations were observed, the local sands have very high FC (Maurer et al., 2015; Taylor, 2015; Green et al., 2014). These observations on high FC sands have much potential for advancing insights on soil liquefaction.

Previous studies have mainly focused on clean sands as few laboratory data were available to support procedural improvements capable of effectively dealing with silty sands. Nevertheless, in recent years, Christchurch sandy soils have been the object of comprehensive laboratory

work (Rees, 2010; Taylor, 2015; Beyzaei et al., 2018; Markham et al., 2018; Cappellaro, 2019). Indeed, Christchurch offers a unique opportunity to investigate the effect of FC on the location of CSL in the $e - p'$ plane. Thus, this paper complements previous research work by proposing a general framework within Generalized Plasticity to assess the liquefaction potential for granular materials with different FC and compares it with the state-of-practice simplified liquefaction assessment procedures.

In the following sections, first, the state-of-practice liquefaction triggering procedures are described. Then, the formulation of the Modified Pastor-Zienkiewicz Generalized Plasticity constitutive law is illustrated along with the mathematical definition for the coupling between the solid and fluid phases of the saturated soil. The CES, and in particular the 2011 Christchurch Earthquake, is used as a case study to compare liquefaction procedures from the simplified approaches and numerical modelling of different configurations of the soil column for different FC. Finally, conclusions are drawn from this analysis.

2. STATE OF PRACTICE PROCEDURES FOR LIQUEFACTION ASSESSMENT

The state-of-practice procedures for the assessment of liquefaction potential are based on simplified relationships derived by correlating liquefaction manifestations with in situ test parameters. The original formulation for this type of analysis was firstly proposed by Seed and Idriss in the early 1970s (Seed and Idriss, 1971) and consisted of analyzing Standard Penetration Test (SPT) in order to differentiate liquefiable from not liquefiable soils. Since then, these simplified correlations have evolved (e.g. Yang et al., 2017; Juang et al., 2012) and adapted in order to consider different soil tests, such as the Cone Penetration Test (CPT), (Youd and Idriss, 2001) or seismic dilatometer Marchetti tests (SDMTs) (Monaco et al. 2005; Grasso and Maugeri 2008; Grasso et al. 2021).

The procedure itself has been standardised in Youd and Idriss (2001) and later updated, for instance, by Idriss and Boulanger (2008) and Boulanger and Idriss (2014), amongst others.

Generally, liquefaction triggering procedures consist of comparing the earthquake-induced Cyclic Stress Ratio (CSR), which represents the seismic demand on a soil layer at a depth z, with the Cyclic Resistance Ratio (CRR), which represents the capacity of the soil to resist liquefaction, to derive a Factor of Safety (FS) against liquefaction triggering. Liquefaction is predicted to occur in a soil layer if FS is less than 1. Liquefaction manifestations at the surface can then be predicted, for instance, through the Liquefaction Potential Index (LPI), (Iwasaki et al., 1978), which corresponds to the integral function of the FS for each soil layer within the upper 20 m of the soil profile analysed as indicated by the formula: $LPI = \int_0^{20m} F(10 - 0.5z)dz$, where $F = 1 - FS$ for a single soil layer of thickness dz and z is the depth of the layer. In this approach, the percentage of FC comes mainly into play for the estimation of the CRR of the soil.

For mathematical convenience, the CRR of the soil is usually expressed in terms of clean-sand values (FC<5%). The CRR can be calculated starting from the blow-count value (N-value) or the measured tip resistance (q_c) obtained as a result of the SPT or CPT tests, respectively. The liquefaction resistance can also be evaluated by the horizontal stress index (KD) from seismic dilatometer Marchetti tests (SDMTs) (Monaco et al. 2005; Grasso and Maugeri 2008; Grasso et al. 2021).

By way of illustration, Fig. 1 shows the CPT-based formulation, according to Idriss and Boulanger (2008). According to this formulation, the q_c at a given depth z is normalised considering the over-burden stress σ'_v and atmospheric pressure P_a, and then is adjusted to a

clean sand value q_{c1Ncs} through a clean-sand parameter Δq_{c1N} to take into account the influence of FC on the penetration resistance.

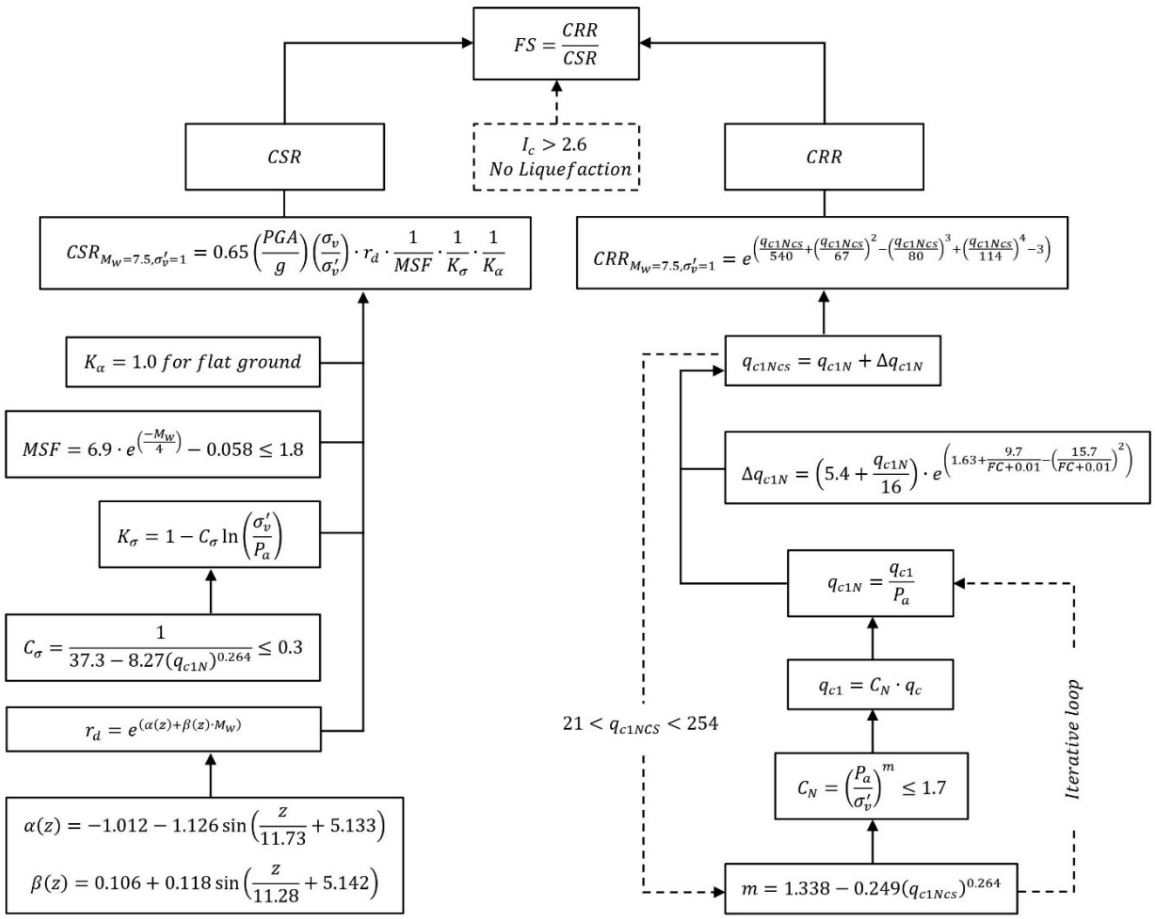

Fig. 1. Liquefaction triggering procedure: Idriss and Boulanger (2008) CPT-based method (Idriss and Boulanger, 2008). Acronyms: CRR, Cyclic Resistance Ratio; CSR, Cyclic Stress Ratio; FC, Fines content; FS, Factor of Safety; MSF, Magnitude Scaling Factor; PGA, Peak Ground Acceleration; C_N, Overburden correction factor; I_c, Soil Behavior Type Index; K_α, Static shear stress; K_σ, Effective overburden stress factor; M_w, Moment Magnitude; m, exponent for the overburden correction factor; P_a, Atmospheric pressure; q_c, measured cone resistance; q_{c1n}, cone penetration resistance corrected for overburden stress effects; q_{c1ncs}, equivalent cone penetration resistance for clean sand; r_d, stress reduction coefficient; $\alpha(z)$ and $\beta(z)$ esponents for the estimation of r_d; σ'_{v0}, effective vertical stress; σ'_{v0}, total vertical stress; z, depth; Δq_{c1n}, clean sand parameter.

The SPT-based approaches follow a comparable approach to the CPT-based ones. Standard Penetration Test (SPT) is a simple in-situ testing to infer the strength of soils. It consists of recording the number of blows required to drive a split-spoon sampler into the ground 15 cm by dropping a calibrated hammer over the sampler from 76cm height. The test finishes once

the total penetration is 45cm. The standard penetration resistance (N_{SPT}) is the number of blows required to penetrate the last 30cm. Cone penetration testing (CPT) is another in-situ test procedure that consists of pushing an instrumented cone penetrometer into the ground at a constant rate. During the test, it is possible to measure the penetration resistance at the tip and the sleeve friction during penetration (Schnaid, 2008).

Independent from the approach adopted, the FC impacts the estimation of CRR as evidenced by Cheng et al. 2019, Prasomsri and Takahasi 2020, Cappellano et al. 2021, or Phan et al. 2021, among many others. These FC values are commonly retrieved from laboratory analysis of borehole samples and correspond to the percentage of fines passing a sieve number 4. In the absence of site-specific soil sampling and lab testing data, FC can also be estimated from the CPT tests using the empirical Robertson and Wride (1998) equations:

$$FC = \begin{cases} 0 & if\ I_C < 1.26 \\ 1.75 \cdot I_C^{3.25} - 3.7 & if\ 1.26 \leq I_C < 3.5 \\ 100 & if\ I_C \geq 3.5 \end{cases} \quad (1)$$

where the Soil Behaviour Type Index I_C (Robertson and Wride, 1998; Youd et al., 2001) is a function of the dimensionless CPT tip resistance, Q, and normalized friction ratio, F:

$$I_c = \sqrt{(3.47 - \log Q)^2 + (1.22 + \log F)^2} \quad (2)$$

$$Q = \frac{q_c - \sigma_v}{P_a} \cdot \left(\frac{P_a}{\sigma_v'}\right)^n \quad (3)$$

$$F = \frac{f_s}{q_c - \sigma_v} \cdot 100\% \quad (4)$$

and where n is in the range of 0.5 to 1.0 as calculated using the Robertson and Wride (1998) method.

3. GENERALIZED PLASTICITY APPROACH

In this paper, simplified methods for liquefaction assessment are compared with numerical approaches based on the generalized plasticity theory.

3.1 Constitutive model

MPZ is a constitutive model within the framework of critical state soil mechanics and generalised plasticity (Pastor et al., 1990; Manzanal et al., 2011a; 2011b; 2010). In the Generalised Plasticity Theory (GPT), introduced by Zienkiewicz and Mroz (1984), and later extended by Pastor et al. (1990), neither yield nor plastic potential surfaces are explicitly defined as mathematical expressions. Instead, their gradients are used in the formulation of GPT.

The MPZ model assumes that the soil seeks an asymptotic critical state when it is sheared. The critical state is defined through the void ratio and the effective confinement stress. It can reproduce the stress-strain behaviour for density conditions either looser or denser than the critical state, thanks to the state parameter, classically defined as shown in Fig. 2.

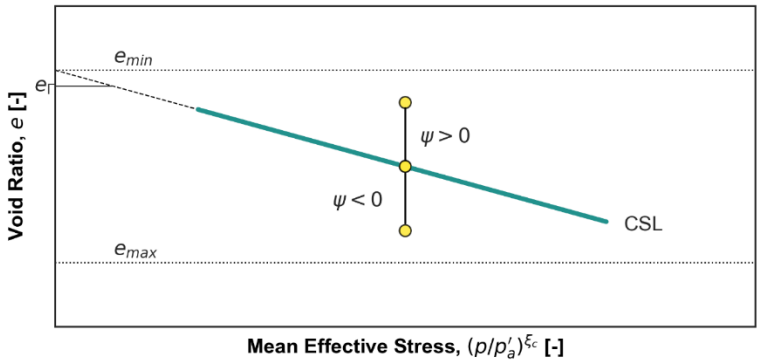

Fig. 2. Definition of state parameter (after Been and Jefferies, 1985).

The most widely accepted state parameter ψ is defined by Been and Jefferies (1985) as the difference of the current voids ratio and the voids ratio at critical state under the same confining pressure:

$$\psi = e - e_c = e_\Gamma + \lambda \left(\frac{p_c^{'}}{P_a'} \right)^{\xi_c} \tag{5}$$

where e_Γ is the critical void ratio at a confining pressure of 1 kPa, λ is the slope of the critical state line in a $e - p'$ plane, $\xi_c$varies between 0.60 to 0.80 as stated by Li (1997); e_c and p_c' are the voids ratio and confining pressure at a critical state, respectively and p_a' is atmospheric pressure.

In the MPZ model, it is assumed that the soil elastic properties depend on the confining pressure p' and voids ratio e as proposed by Richart et al. (1970), the bulk modulus K and the shear modulus G are defined as:

$$K = K_{evo} \cdot \frac{(2.97 - e)^2}{1 + e} \cdot \sqrt{p' \cdot p_a'} \tag{6}$$

$$G = G_{eso} \cdot \frac{(2.97 - e)^2}{1 + e} \cdot \sqrt{p' \cdot p_a'} \tag{7}$$

where G_{eso} and K_{evo} are dimensionless material parameters.

The elements characterising the plastic strain increment are defined as follows:

$$d\boldsymbol{\varepsilon}^p = \frac{1}{H_{L/U}} \left(\boldsymbol{n}_{gL/U} \otimes \boldsymbol{n} \right) : d\boldsymbol{\sigma} \tag{8}$$

where $\boldsymbol{n}_{gL/U}$ represents the unit vector perpendicular to the plastic potential surface, under loading (L) or unloading (U) conditions, $\boldsymbol{n}$ is the unit vector perpendicular to the yield surface and $\otimes$ denotes their vector product.

The direction of the plastic flow is obtained from laboratory tests as a function of dilatancy d_g:

$$\boldsymbol{n}_g = \left(\frac{d_g}{\sqrt{1+d_g^2}}, \frac{1}{\sqrt{1+d_g^2}} \right)^T \qquad d_g = \frac{d_0}{M_g} \cdot \left(M_g \cdot e^{m\psi} - \eta \right) \tag{9}$$

and where d_0 and m are model constants; ψ is the state parameter defined by equation (5); η is the stress ratio and M_g is the slope of the Critical State Line in the $p' - q$ plane.

A similar expression to that derived under unloading conditions, $\boldsymbol{n}_g$, is adopted for determining the loading-unloading discriminating direction tensor $\boldsymbol{n}$:

$$\boldsymbol{n} = \left(\frac{d_f}{\sqrt{1+d_f^2}}, \frac{1}{\sqrt{1+d_f^2}} \right)^T \qquad d_f = \frac{d_0}{M_f} \left(M_f \cdot e^{m\psi} - \eta \right) \tag{10}$$

where:

$$\frac{M_f}{M_g} = h_1 - h_2 \left(\frac{e}{e_c} \right)^{\beta} \tag{11}$$

and h_1, h_2 and β model constants.

The plastic modulus for loading is postulated directly without introducing any hardening law and consistency condition, as:

$$H_L = H_0' \cdot e^{-\beta_0' \left(\frac{e}{e_c} \right)^{\beta}} \sqrt{p' \cdot P_a'} \cdot H_{DM} \cdot H_f (H_v + H_s) \tag{12}$$

where H_0' and β_0' are model parameters for isotropic loading. H_f, H_{DM} H_v, and H_s are defined by the following equations:

$$H_f = \left(1 - \frac{\eta}{\eta_f}\right)^4 \qquad \eta_f = \left(1 + \frac{1}{\alpha_f}\right) \cdot M_f \tag{13}$$

$$H_{DM} = \left(\frac{\xi_{MAX}}{\xi}\right)^{\gamma} \qquad \xi = p'\left[1 - \left(\frac{\alpha}{1+\alpha}\right) \cdot \frac{\eta}{M_f}\right]^{-1/\alpha} \tag{14}$$

$$H_v = H_{v0}\left[M_g \cdot e^{-\beta_v \psi} - \eta\right] \qquad H_s = \beta_1 \cdot e^{-\beta_0 \cdot \xi_{dev}} \tag{15}$$

where $H_{v0}, \beta_v, \beta_0, \beta_1, \gamma$ are parameters of the model. ξ_{dev} is the accumulated deviatoric plastic strain.

The law suggested for the unloading plastic modulus assumes that there are plastic strains from the beginning of the unloading process, and it is proposed to be of the form:

$$H_u = H_{u0}\left(\frac{M_g}{\eta_u}\right)^{\gamma_u} for \left|\frac{M_g}{\eta_u}\right| > 1 \tag{16}$$

$$H_u = H_{u0}\, for \left|\frac{M_g}{\eta_u}\right| < 1 \tag{17}$$

where H_{u0} and γ_u are constitutive parameters and η_u, referred to as the unloading stress ratio is the stress ratio from which unloading takes place.

3.2 Numerical model

A mathematical model for reproducing the interaction between the soil skeleton and the pore fluid in a saturated layer was first proposed by Biot (1941) for elastic linear elastic materials. This was extended by Zienkiewicz et al. (1980; 1990) for non-linear materials: drained, undrained, consolidating, and dynamic behaviour assumptions in soils. These equations represent the equilibrium of the solid and fluid phases and the continuity of flow. At every

point of the domain, the degrees of freedom are the vector of the displacements of solid and fluid phases (with three components each in a 3D problem), as well as the pore water pressure. Several successful attempts have been made to reduce the number of degrees of freedom when the Biot's equations are implemented in a numerical scheme (Zienkiewicz et al., 1999; Zienkiewicz and Shiomi, 1984; Ghaboussi and Wilson, 1973). The most widely used is the so-called $u - p_w$ formulation, which is based on the assumption that the relative acceleration between fluid and solid is negligible. In this formulation, the number of degrees of freedom in every node is reduced to the vector of displacements in the soil and the pore water pressure, (i.e. four in each node, in a 3D model). Another formulation, which does not require any additional assumptions, is the $u - w$ formulation which computes the vector of solid displacement and relative displacement of fluid respect to the solid phase), (López-Querol et al., 2008). In this case, the displacements for solid and fluids phases are calculated in each node (six in total). In this study, the coupled $u - p_w$ formulation is used to represent the interaction between the soil skeleton and pore fluid. If the shape functions for the displacement and pore pressure fields are not adequately designed, this formulation may produce results with numerical instabilities in the undrained incompressible limit. A saturated medium is said to be in the undrained incompressible limit when it combines a quasi-incompressible mix (solid + fluid) with a quasi-undrained condition associated with low permeability. The standard shape function design (Zienkiewicz et al., 1999), which is used here provides a stable formulation, and is a combination of quadratic shape functions for the displacement field and linear shape functions for the pore water pressure field. If the same degree of interpolation is used for both fields, stabilisation algorithms might be required to avoid spurious numerical instabilities in the solutions (Biot, 1941; Li, 1997).

The numerical formulation used in this study is based on a space discretisation stage of the mathematical model equations, carried out using the shape function design and standard

residual Galerkin techniques. This first stage is followed by discretisation in time, which is performed based on a Generalised Newmark expansion with a GN22 format for displacements and a GN11 format for pore pressures. Finally, the non-linearity of the problem requires to set up a Newton-Raphson framework to obtain a solution iteratively. A detailed description of this numerical formulation may be found in Chapter 3 of Zienkiewicz et al. (1999).

4 CASE STUDY

4.1 Christchurch (New Zealand)

The city of Christchurch is chosen as a case study due to the unprecedented size and detail of geotechnical data available. More than 30,000 CPT and approximately 18,000 SPT tests were performed after the CES and can be downloaded from the NZGD (Ministry for Business Innovation & Employment, 2018). Additional laboratory tests performed using the triaxial apparatus at the University of Canterbury are also freely available (Taylor, 2015), which allow very accurate characterisation of liquefaction potential of sand with fines in the analysed site (Kilmore Street Site, K1, see Fig. 3).

The sandy soils underlying Christchurch are highly susceptible to liquefaction during a high magnitude earthquake. Indeed, liquefaction is a long-established risk for Christchurch (Brackley, 2012). Historical liquefaction manifestations were observed at the estuary of the Avon and Heathcote rivers in 1869 and coastal areas north of Kaiapoi during the Cheviot earthquake in 1901 and Motunau earthquake in 1922 (Brackley, 2012). Liquefaction manifestations were also reported after each earthquake of the CES. Amongst them, the 22nd of February 2011 earthquake ($M_w = 6.2$), which is adopted in this paper as a case study, is currently one of the most extensive liquefaction manifestation events on record (Maurer et al., 2014). This event was induced by a strike-slip rupture on a formerly unrecognised fault that

has been located 10 km to the southeast from the city centre, at a depth of 5-6 km (Beavan et al., 2011). Due to the shallow depth of the earthquake and its proximity to the city centre, very high ground motions were registered by the 33 recording stations placed around the Christchurch area. As indicated by the recordings obtained from PEER Ground Motion Database (Ancheta et al., 2014), the highest Peak Ground Acceleration (PGA) recorded was 1.41g at Heathcote Valley Primary School (roughly 2.4 km from the epicentre). As a result, unprecedented levels of liquefaction were surveyed across a wide area in the suburbs north to south of the city, and northeast along the River Avon (New Zealand Geotechnical Database, 2013).

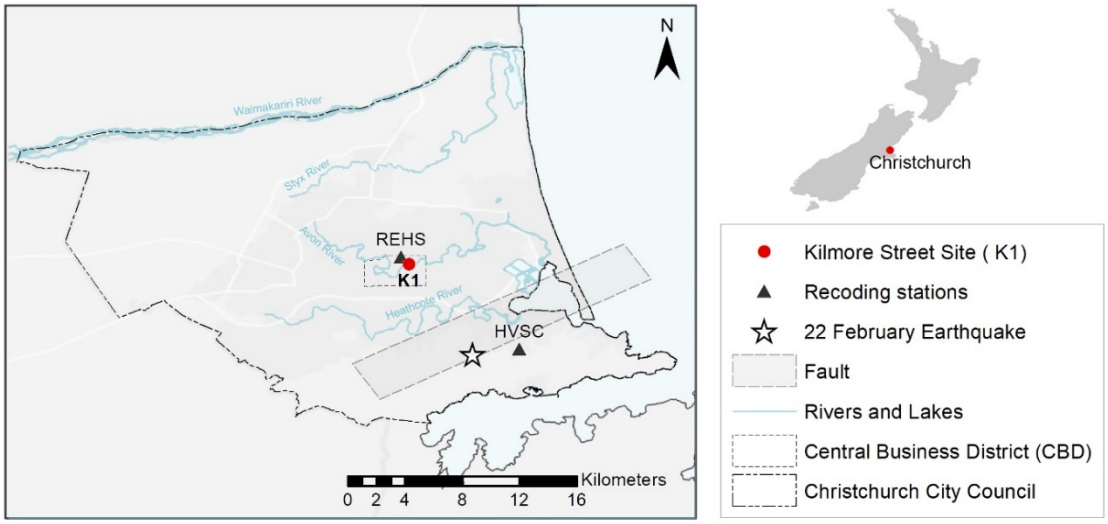

Fig. 3. Location map (in WGS84 coordinate system) of the Kilmore street Site (K1), Heathcote Valley Primary School (HVSC) and Christchurch Resthaven (REHS) recording stations, the 22nd February Earthquake and correspondent fault system (adapted from Beavan et al., 2011).

Lateral spreading, sand boils, settlement, silt mud ejections and water ponding on the ground surface observed after the Christchurch event are consistent with the geology of the area. The soil on which the Central Business District (CBD) lies has a recent formation (Bertelli et al., 2019). The basement rock and the volcanic rocks that form the current Bank peninsula originated, from the Permian-Cretaceous Period and Miocene Epochs, respectively. It is only during the cycles of glaciations that characterised the last part of the Quaternary Period that the

Canterbury Plain formed through interfingering of river gravels eroded from the basement rocks of the Canterbury foothills and the South Alps with fine-grained shallow marine and coastal sediments as shown in Fig. 4 (Brown and Weeber, 1992). Consequently, a substantial area of Christchurch is underlain with sands that are susceptible to liquefaction.

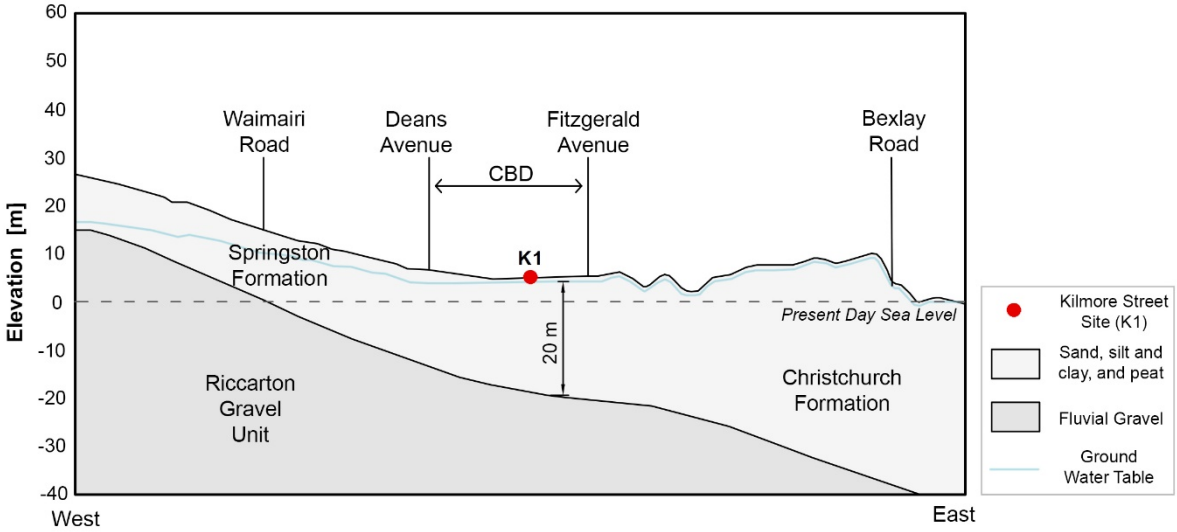

Fig. 4. Schematic geologic section of Christchurch (after Brown and Weeber, 1992) with the location of the Kilmore Street site K1 and the Central Business District (CBD).

Regarding the mineralogy of these upper sandy soil layers, there are no differences between marine sands of the Christchurch Formation and the fluvial sands of the Springston (Taylor, 2015). Indeed, as reported by Taylor (2015), the Christchurch Formation sands are clean, moderately spherical particles, sub-angular to sub-rounded in shape. In contrast, Springston Formation silty sands exhibit sub-angular slightly spherical particles with the fines having a more angular shape. Scanning Electron Microscope images of a typical fluvial silty sand and clean marine sand from K1 is shown Taylor (2015). The sand-sized particles are coated in

fines and do not appear as 'clean' particles under the microscope. The fine sized particles ($< 75\mu m$) range from moderately spherical in shape for the larger particles, to more angular, elongated and some plate-like for the smaller fines. Also, the median grain size D_{50} of the Christchurch Formation sands (FC < 5 %) is approximately between 0.2 and 0.3 mm, with a coefficient of uniformity c_u varying between 1.9 and 3.4, while for the Springston Formation silty sands and sandy silts (FC 13 –98 %) D_{50} varied between 0.03 and 0.14 mm, c_u between 2.3 and 6 (Taylor, 2015).

The described geological process also influences the current hydrological system as the Canterbury Plain mirrors the flow regime of the rivers which deposited the sediments (Beyzaei et al., 2018)(Taylor, 2015). Gravelly materials prevail in western areas of the plain, whereas sands through clays are more prevalent towards the cost. Similarly, the Ground Water Table (GWT) lies several meters or more below the surface, and it rises to the surface closer to the coast. Its fluctuation is evident in Christchurch itself where the GWT is at approximately $2 - 3\ m$ depth in the western suburbs and $0 - 2\ m$ in the eastern ones (Maurer et al., 2014). As a result, these hydraulic and geologic features increase the susceptibility of Christchurch soils to undergo liquefaction during major seismic events, as it is well known that sandy soils are required to be saturated to liquefy.

4.2 144 Kilmore Street

A soil column corresponding to 144 Kilmore Street Site (-43.5264, 172.6400 in WGS84 coordinate system; Taylor, 2015) - K1 Site from hereon - is chosen to be analysed in detail to investigate the influence of the FC on both simplified and numerical liquefaction prediction methods. This location has the potential to suffer both liquefaction and lateral spreading, as it is situated immediately north of the Avon River (Taylor, 2015). Before the CES, the site was occupied by a single-family residential building, and so it can be assumed as a level, free-field

ground. The upper 8 m of the soil column comprises loose to medium dense grey finely interbedded silty fine sands and sandy silts (reworked flood over-bank deposits), with non-plastic fines contents of 120 mm high specimens predominantly between $15 - 50\%$. Below $8m$, medium-dense and then dense brown clean medium sands (marine beach/dune sands) are encountered up to 22 m depth. Thus, the first 8 m of the soil column can be assumed to belong to the Springston formation, whereas the more profound depths before reaching the Riccarton Gravel Unit to the Christchurch formation (Taylor, 2015).

The Christchurch earthquake caused extensive and severe liquefaction at this site (Taylor, 2015). The closest recording station from K1 was the Christchurch Resthaven REHS (-43.522, 172.635 in WGS84 coordinate system, roughly 7.8 km from the epicenter), which recorded a PGA of $0.71g$ on the Southeast component accelerogram (Fig. 5), (Ancheta et al., 2014). The February 2011 reconnaissance investigation map (New Zealand Geotechnical Database, 2013) classify the liquefaction manifestation at the site as 'severe', with no lateral spreading but with large quantities of ejected material. The sand ejecta has been identified as being from the grey fluvial silty-sand materials originating in the upper 8 m soil profile (Taylor, 2015).

Further insights on this soil column are presented in Section 4.5 of this paper.

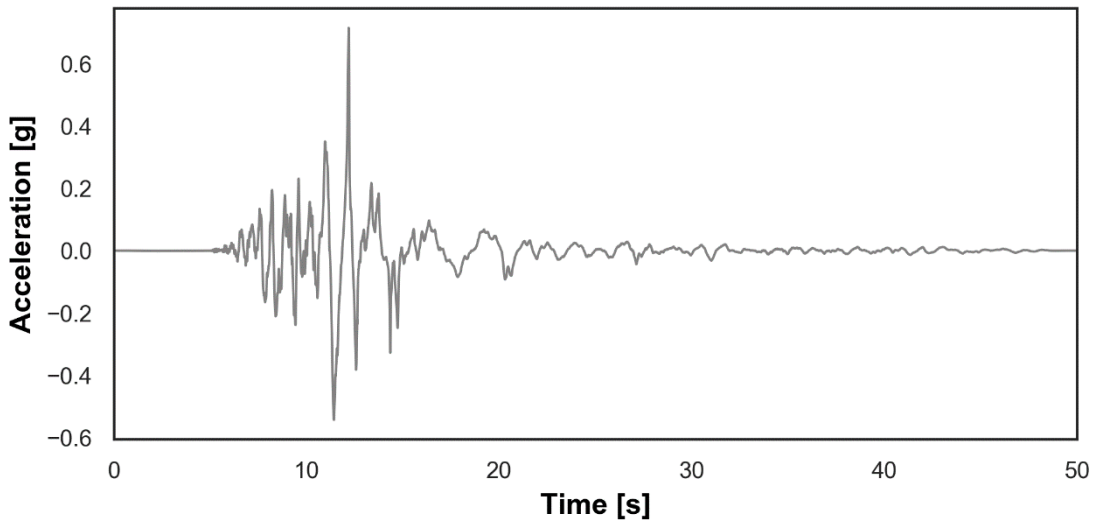

Fig. 5. Christchurch Resthavent (REHS) Recording station, 22 February 2011 event, South-East Component. Peak acceleration value: 0.71g (Ancheta et al., 2014).

4.3 Simplified procedures

Through the NZGD (Ministry for Business Innovation & Employment, 2018), 54 high-quality investigation sites spread across the entire municipal territory are selected to compare the different liquefaction triggering methodologies. These sites are chosen based on the availability of both CPT and SPT measurements at the same location, termination depth over $10\,m$, proximity to ground motions recording stations, and availability of piezometer readings to estimate the fluctuation of the GWT over time. For each of these locations, the tests available from the NZGD correspond to a borehole report, FC estimation report, raw CPT log, and instruments specifications.

In order to estimate the Factor of Safety (FS) against liquefaction associated with all the selected CPT/SPT soil profiles, the simplified relationships reported by Youd and Idriss (2001), Idriss and Boulanger (2008), Boulanger and Idriss (2014) are adopted. For both CPT-based and SPT-based, the model selection includes a combination of four models from Youd & Idriss (2001) with MSF from Idriss (1995) or Andrus & Stokoe (1997), and reduction coefficients

r_d from Blake (1996) or Idriss (1999), respectively as reported in Youd & Idriss (2001); then the Idriss & Boulanger (2008)'s model, and the Boulanger & Idriss (2014) one. It is noted that different relationships from different authors have not been combined with the only exception of the model of Youd & Idriss (2001) where the different alternatives have been made available by the authors themselves. For the application of these relationships, soil unit weights are presumed to be 17 $kN/m3$ above the GWT, and 19.5 $kN/m3$ below the GWT, as they are representative values for the soils in this location (Wotherspoon et al., 2014). The PGA at each site is instead extrapolated from a "Conditional PGA for liquefaction assessment" map developed for conventional liquefaction assessments by Bradley Seismic Ltd. and the University of Canterbury (New Zealand Geotechnical Database, 2015). For the CPT-based methodology, the FC are estimated using the Robertson and Wride (1998) method as reported in equation (1); this provides a continuous FC estimate along with the depth of the soil profile, as the FC estimated from laboratory analysis are scarce and might not be representative of all different soil layers. Finally, for the estimation of LPI values, soil layers are considered to be potentially liquefiable if I_c is less than 2.6 (Youd and Idriss, 2001;Idriss and Boulanger, 2008; Boulanger and Idriss, 2014).

For the current research, "Liquefaction and Lateral Spreading Observations" of property or road maps (New Zealand Geotechnical Database, 2013) is adopted as a reference for comparison. This source provides the most reliable information currently available on the NZGD as they classify the observed liquefaction as none, minor, moderate, severe, moderate-to-severe, very severe based on the evidence and quantity of ejected material as well as the lateral displacement visible at the ground surface.

A spatial-analysis correlation is then established between the calculated LPI values and the observed liquefaction manifestations reported in the aforementioned maps. In order to do this,

the prediction of liquefaction occurrence is reduced to a binary system. For this purpose, the lower band of the Iwasaki Criterion (Iwasaki et al., 1984) is assumed to identify the occurrence of liquefaction; as such, if $LPI \geq 5$ liquefaction manifestations are expected at the investigated site. Likewise, the maps of liquefaction observations are reinterpreted by re-classifying each site as "No Liquefaction" or "Liquefaction"; where the "none" and "minor" classes are mapped as "No Liquefaction", and all other classes as "Liquefaction." The simplified approaches' predictions of liquefaction are compared to the observations using a confusion matrix approach, where True-Positive (TP) indicates a correct-prediction of observed liquefaction occurrence. True-Negatives (TN) indicates a correct-prediction of observations of no liquefaction. False-Positive (FP) represents the case when liquefaction is predicted by the simplified methods but is not observed to occur. False-Negative (FN) represents the case when liquefaction is not predicted to occur by the simplified methods but is observed in the maps. Based on a confusion matrix classification, exploratory spatial analysis is carried out to evaluate the overall LPI performance of the tested SPT-based and CPT-based approaches, as shown respectively in Fig. 6a and Fig. 6b.

(a)

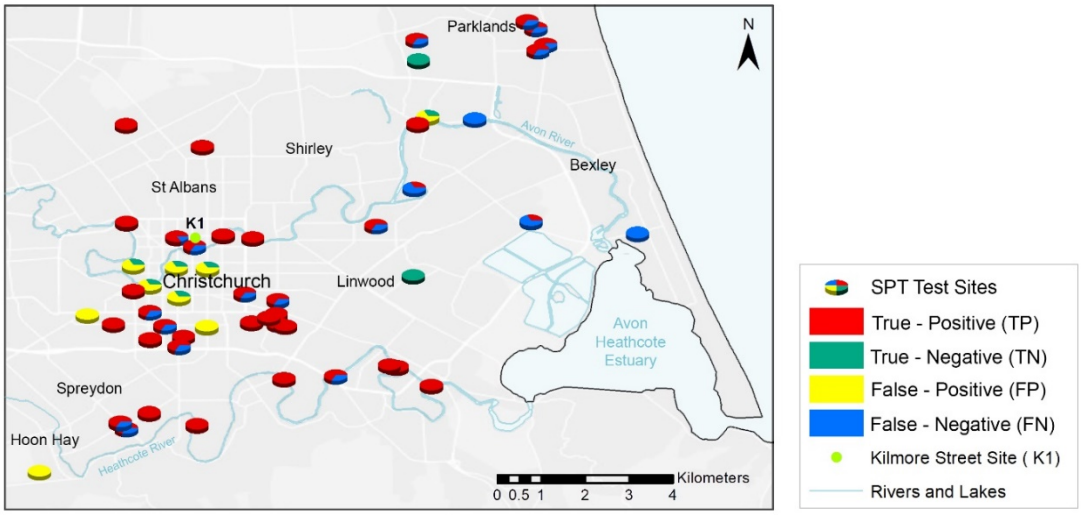

(b)

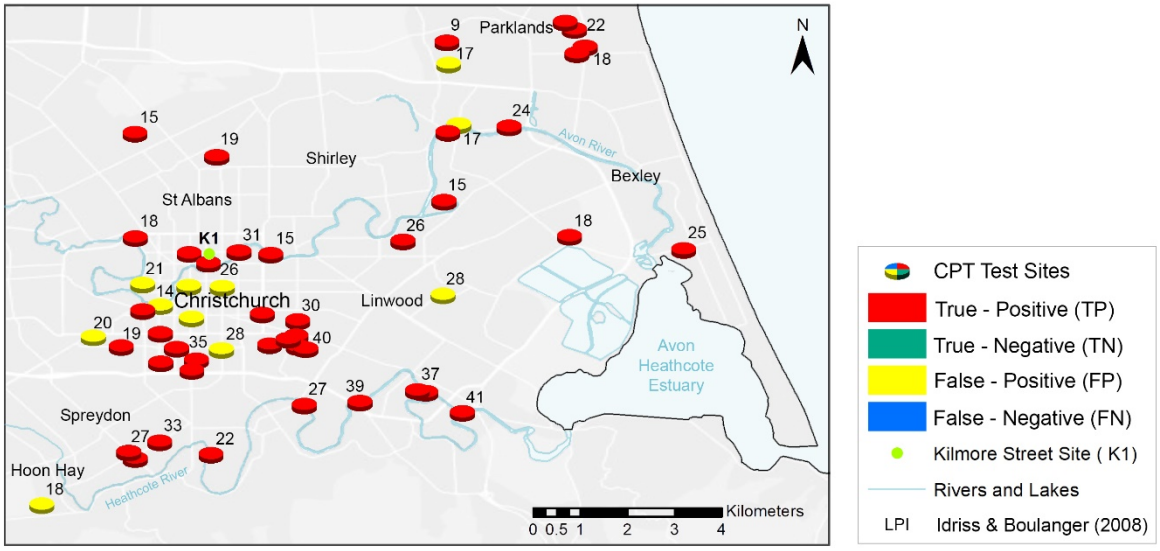

Fig. 6. Comparison of the observation data with the LPI values (WGS84 coordinate system): a) SPT-based approach; b) CPT-based approach.

Taken together, Fig. 6.a and Fig. 6.b show an over-prediction of liquefaction by the simplified methods. The pie-charts adopted for symbolising the cumulative results from the twelve different methodologies at each test location are predominantly "yellow", i.e. "False-Positive", in the westerns suburbs of Christchurch. This inconsistency between the predictions and observations might be due to the geomorphological features of this area. This is particularly

evident for the CPT-based methodologies. The increasing mix of sand, silt and gravel in these soil profiles would have misled the calculation of I_c factors, and thus lower FC estimation, which in turn results in higher LPI values and leads to an overprediction of liquefaction manifestations.

Regarding the differences between methodologies, CPT-based ones result in being overall more accurate. At the location in central Christchurch with liquefaction manifestations, the CPT-based methodology consistently predicts the occurrence of liquefaction, i.e. "True-Positive". Instead, the SPT-based provide much more variability of results; they correctly predict the non-occurrence of liquefaction manifestations near Linwood ("True-Positive"), but also greatly underpredicting the occurrence of liquefaction in central Christchurch (i.e. "False – Negative" for Kilmore Street site). The comparison between the CPT-based and SPT-based methods for the Kilmore Street site indicates that all the six CPT-based procedures correctly predicted the occurrence of liquefaction at the site, whereas the two most recent SPT-based procedures do not predict the occurrence of liquefaction at the site. A possible explanation for this result may be the lack of FC values for different soil layers in the retrieved boreholes; FC estimations used for the SPT tests do not offer continuous data in contrast with the CPT tests when using eq. (*1*).

Taken together, a remarkable aspect of these simplified methods is that the results from different formulations are similar; they all tend to be conservative as they over-predict liquefaction occurrences. This can be seen by analysing the CPT profile of the K1 Site represented in Fig.7, which summarises the LPI evaluation through the CPT-based by Idriss and Boulanger (2008). Indeed, Fig.7 shows that liquefaction is predicted from roughly $2\ m$ to $16\ m$ depth w, which could agree with the extensive ejected material observed at the site after the Christchurch event (New Zealand Geotechnical Database, 2013). However, the FC

estimated through the Robertson and Wride (1998) formula, is much lower than the FC determined from laboratory analysis (Taylor, 2015), which decreases the CRR of the soil profile. Thus, the obtained LPI is likely to be an over-prediction of liquefaction at the site and can be related to the significant uncertainties in the I_c versus FC empirical relationship (Boulanger and Idriss, 2014).

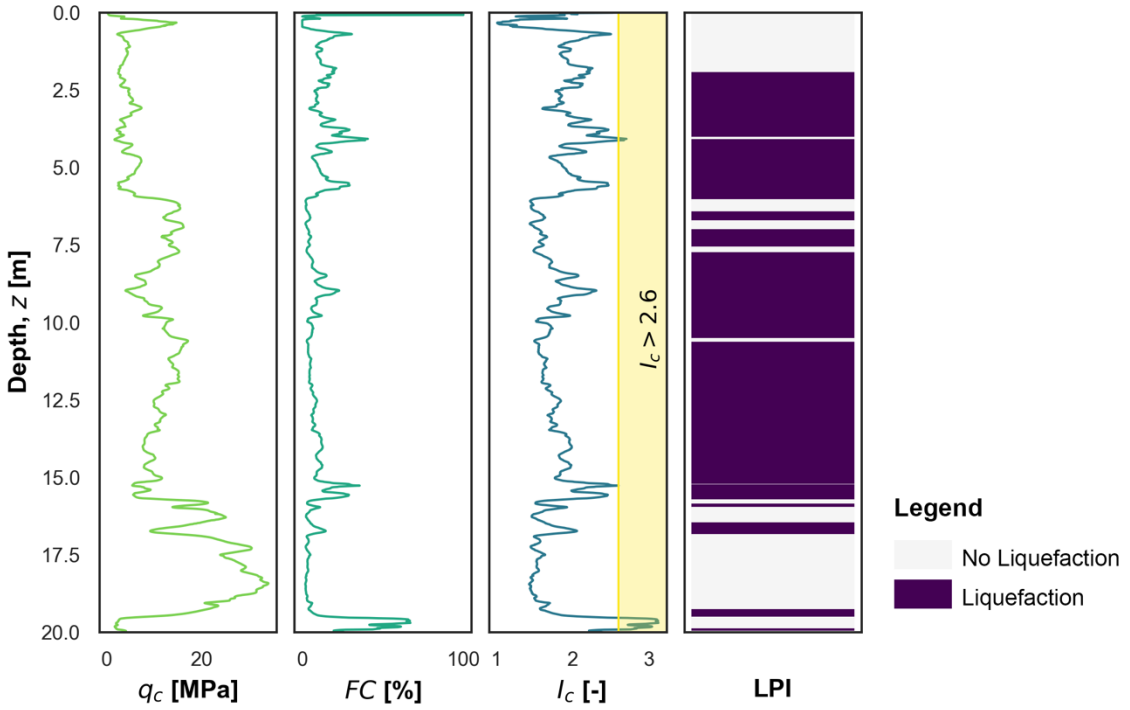

Fig.7. CPT-based liquefaction triggering assessment: a) q_c values; b) FC estimation and c) Soil Behaviour Type Index Ic d) Identification of potentially liquefiable layer through Idriss and Boulanger (2008).

4.4 Numerical approach: Calibration of the constitutive model

To assess the suitability of the selected constitutive model, it is calibrated with experimental results obtained from the Springton and Christchurch formation (Taylor, 2015). As mentioned, the material was collected from a geotechnical campaign at K1 Site (Fig. *6*). This street was

severely affected by liquefaction-induced ground deformation in the last earthquake events in the CBD. In the conducted site and laboratory characterisation, loose to medium dense grey silty fine sands and sandy with non-plastic FC predominantly between 15 – 50 % were found over the upper $8\,m$. Below this, medium-dense and then dense brown clean medium sands were encountered to a 22 m depth, where the gravels shown in Fig. 4 (as reported by Taylor, 2015) appeared. All analysed samples have been isotropically consolidated and then sheared under confining pressures between 50 kPa and 200 kPa and void ratios between 0.722 and 1.05. Table 1 shows the initial value of void ratio and effective confining pressure of the calibrated undrained triaxial tests for different FC. The nomenclature adopted by Taylor (2015) to identify each sample tested (K1-X-SX-UX) has been maintained to have better traceability of the calibrated tests. K1 is associated with Kilmore Street site, X is the tube number, SX is the sample number, and UX is the undrained triaxial number.

Table 1. Initial conditions of the analysed undrained triaxial test for different fines content (FC), voids ratio (e) and confinement stress ($\boldsymbol{p'}$) (Taylor, 2015)

FC 3%	$\boldsymbol{e}$**[-]**	$\boldsymbol{p'}$**[kPa]**
K1-5-S5-U3	0.774	198.7
K1-5-S5-U2	0.952	49.8
K1-6-S1-U2	0.901	101.6
K1-6-S1-U3	0.957	50.1
FC 17%	$\boldsymbol{e}$**[-]**	$\boldsymbol{p'}$**[kPa]**
K1-4-S4-U3	0.813	201.418
K1-4-S4-U7	0.931	101.418
K1-4-S2-U2	0.963	51.773
FC 40%	$\boldsymbol{e}$**[-]**	$\boldsymbol{p'}$**[kPa]**
K1-2-S4-U4	0.722	299.473
K1-2-S4-U7	0.891	101.23
K1-2-S4-U1	1.053	50.615
FC 58%	$\boldsymbol{e}$**[-]**	$\boldsymbol{p'}$**[kPa]**
K1-3-S1-U1	0.899	99.838
K1-3-S1-U2	0.938	49.919

In all these cases, a single set of constitutive parameters for Christchurch Sand and Springston Silty Sand have been obtained, which are used for all densities, confining pressures, loading path and drainage conditions. Although in the literature it is observed that elastic constants have some variability in testing mixtures of sands with different non-plastic FC (Ratman & Dafalias 2014, Goudarzy et al. 2016), in the case of Christchurch soils where the fines content varies along with the depth for a single site K1, that variability of the elastic parameter is very low as shown by Taylor (2015). Table 2 shows the parameters adopted. G_{eso} and K_{evo} are dimensionless elastic constants given by equation (6) and (7), d_0 and m are model constants related to dilatancy d_g given by equation (9). h_1, h_2 and β are model constants related with loading-unloading discriminating direction tensor $\boldsymbol{n}$ allowing non-associative flow rule. H_0' and

β_0' are a model parameter related to plastic strains at the beginning of the loading process. H_{v0}, β_v, are parameters of the model obtaining the peak stress ratio η_p as a function of the state parameter ψ (equation 15). Details of the parameter calibration can be found in Manzanal (2008) and Cuomo et al. (2018). The suitability of the MPZ constitutive model is explored under monotonic loading.

Table 2. Model parameters after calibration for two different soils.

Parameter		Silty Sand/Clean Sand
Elasticity	G_{eso}	125
	K_{evo}	167
Plastic flow	d_0	0.88
	m	3.5
	h_1/h_2	1.31 /0.85
	β	1.8
Plastic modulus	H_0'	125
	β_0'	1.9
	H_{v0}	175
	β_v	1.5

The critical state lines for different FC and the initial state of the tests are shown in Fig. 8, according to the experimental data reported by Taylor (2015). The critical state parameters obtained from the experimental data for different ranges of fines content ($\boldsymbol{FC}$) and average fines content ($\boldsymbol{FC_{ave}}$) are shown in Table 3. M_g is the slope of the Critical State Line in the $p' - q$ plane, and e_Γ is the critical void ratio at a confining pressure of 1 kPa, λ is the slope of the critical state line in a $e - p'$ plane, ξ_c is a calibration parameter. It is observed that the CSL moves downwards as the FC increases (Fig. 8). The critical void ratio decreases as particle size distribution improve (Poulos, 1981; Sadrekarimi, 2013). The slope of the critical state line increases slightly. In the Springston formation, this behaviour is observed in the range of FC from 3% to 40%. For FC higher than 40%, the critical void ratio increases, and a significant increase in λ is observed.

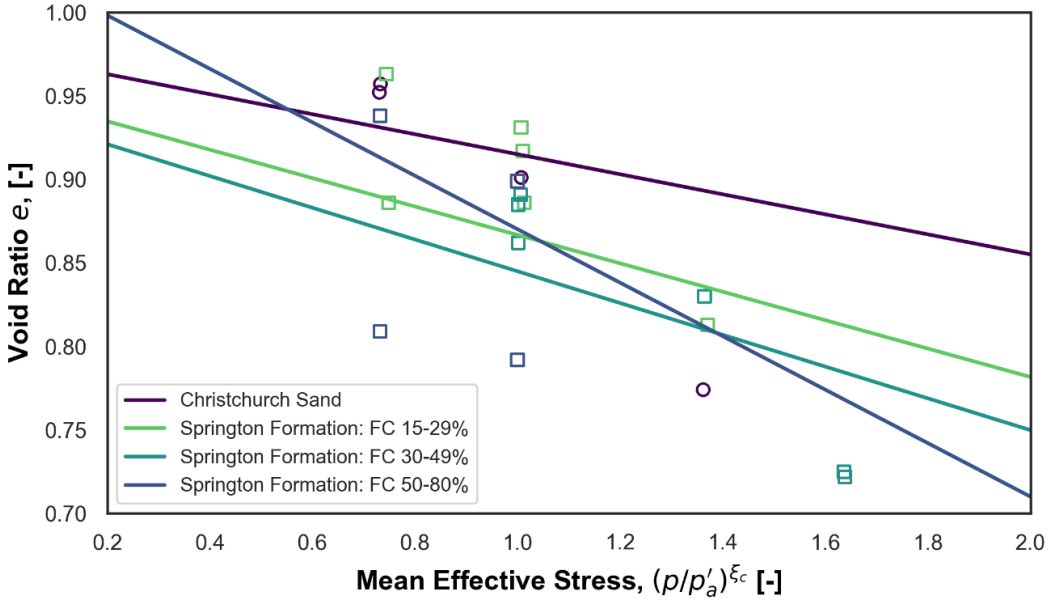

Fig. 8. CSL of the materials for different FC.

Table 3. Critical state parameters for the different range of fines content ($\boldsymbol{FC}$) and average fines content ($\boldsymbol{FC_{ave}}$)

$\boldsymbol{FC}$	$\boldsymbol{FC_{ave}}$	$\boldsymbol{M_g}$	$\boldsymbol{e_\Gamma}$	$\boldsymbol{\lambda}$	$\boldsymbol{\xi_c}$
less 5% (Christchurch Sand)	5	1,38	0,9750	0,060	0,47
15-29%	20	1,38	0,9520	0,085	0,45
30-49%	40	1,38	0,9400	0,095	0,45
50-80%	65	1,38	1,0300	0,160	0,45

Fig. 9 compares the calibration result for undrained triaxial tests in terms of effective stress paths ($q - p'$) for medium dense and loose samples. MPZ model reproduces static liquefaction stress path in loose samples and the contractive – dilative behaviour in medium dense sands with a set of model constants, as shown in Table 2. Fig. 10 presents the calibration for undrained

triaxial tests in terms of effective stress paths ($q - p'$) and stress-strain behaviour for saSpringtonFm silty sand samples with different fine content, ranging from 17 to 58% for the loose and medium dense state.

Remarkably, there is very little difference between the silty sand behavior with different FC and the clean sand. Higher FC does not prevent liquefaction if the initial state of the soil (in terms of its voids ratio and confining stress) yields over the CSL in the plane $e - (p'/p_a)^{\xi}$I.e., there is contractive behaviour in loose sands, for which the state parameter is positive. In such cases, static liquefaction is observed despite the FC. The MPZ model can reproduce this observed behaviour.

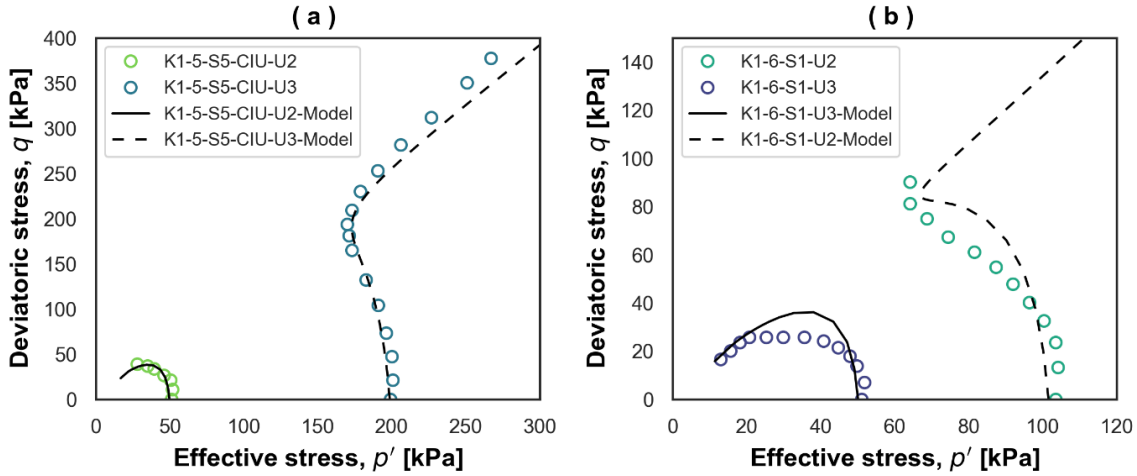

Fig. 9. Calibration results for undrained triaxial tests on Christchurch sand with fines contents 3% for a) confining pressure of 50 and 200 kPa and void ratios of 0.952 and 0.774 respectively and b) confining pressure of 50 and 100 kPa and void ratios of 0.957 and 0.901, respectively. Symbols: experimental data. Lines: model simulations.

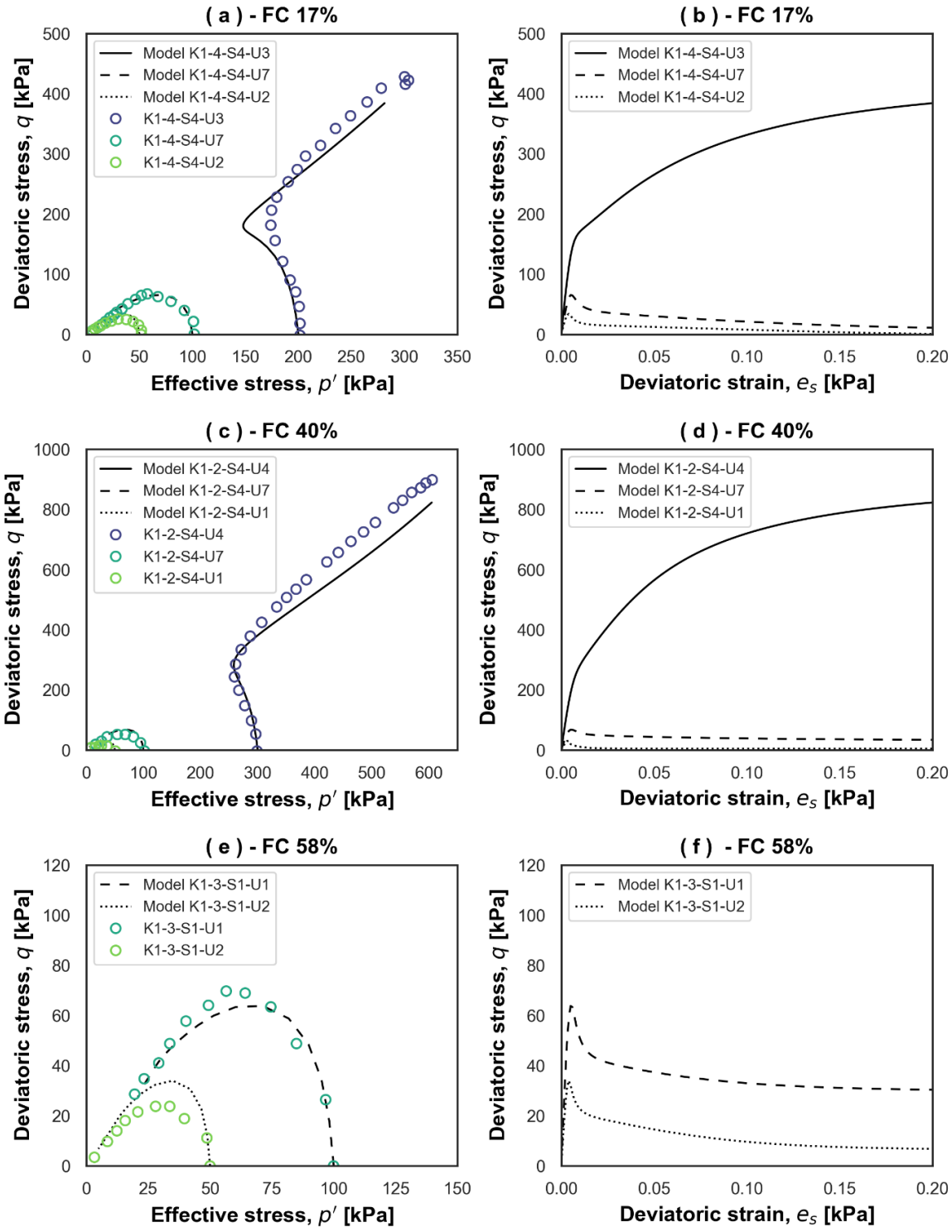

Fig. 10. Comparison of undrained triaxial test and model simulation on Sprinton Fm silty sand for 17, 40, and 58% of fines content for different confining pressure and void ratios. Symbols: experimental data. Lines: model simulations.

4.5 Numerical simulation of the soil column under seismic loading

In order to assess the liquefaction potential of the aforementioned fully saturated soil profile, a finite element model is created in the code GeHoMadrid (Fernandez Merodo et al., 2004) to represent the soil to a depth of $20\,m$ subjected to a horizontal earthquake. The $20\,m$ soil column is divided by an upper silty-sand layer of 8 m and a lower clean sand layer of $12\,m$ (Fig. 11). The seismic input is the SE component accelerogram for the Christchurch case measured at REHS (-43.5015, 172.021 in WGS84 coordinate system) location (Ancheta et al., 2014), (Fig. 5). Both sides and the bottom of the column are assumed impermeable. Pore pressures are assumed to be zero at the surface of the layer. The finite element model consists of 20 standard $u - p_w$ quadrilateral elements, where quadratic shape functions with eight nodes for displacements field variable, and linear shape functions with four nodes for pore pressure field variable, are used. The lateral nodes have repeated boundary conditions, where the displacement of a right-hand side node equals that of the corresponding left-hand side node (Fernandez Merodo et al., 2004). The material parameters used for both silty-sand and clean sand are shown in Table 2.

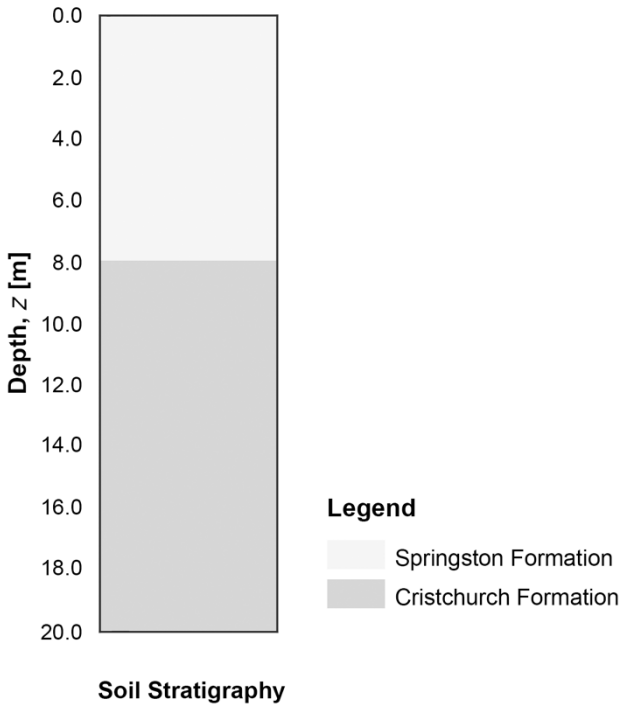

Fig. 11. Schematic column of the studied soil stratigraphy.

This study analyses the effect of the void ratio of the different layers and the effect of fines content on liquefaction susceptibility. Regarding the void ratio effect, different initial conditions for Springston Formation silty sand in the upper $8\,m$ and Christchurch formation clean sand in the lower $12\,m$ of the soil column are numerically modelled. The soil is assumed to have the same initial conditions of the laboratory test calibrated previously for the FC of 17% and 40%. Table 4 summarises the cases studied.

Table 4. Analysed cases for different initial void ratios (e_0) and fines content (FC)

	Upper layer		Lower layer	
Column	$\boldsymbol{e_0}$	$\boldsymbol{FC}$[%]	$\boldsymbol{e_0}$	$\boldsymbol{FC}$[%]
Case Ia	1.030	15-29	0.825	1-5
Case Ib	0.886	15-29	0.825	1-5
Case Ic	0.886	15-29	0.957	1-5
Case IIa	0.960	30-49	0.825	1-5
Case IIb	0.903	30-49	0.825	1-5
Case IIc	0.886	30-49	0.825	1-5
Case IId	0.771	30-49	0.825	1-5

The results for all cases during the earthquake motions are presented in Fig. 12 and Fig. 13, as isochrones lines, which can be compared with the initial vertical effective stress throughout the soil column. It is worth remarking that liquefaction is predicted at those locations where the isochrones touch the initial effective stress line. The evolution of the excess pore pressures for three different times, in conjunction with effective vertical stress for case I, is shown in Fig. 11. After $10\ s$ of loading, the excess pore water pressure equals the initial vertical effective stress leading to the liquefaction of all the upper layer ($8\ m$) with silty sand at loose state (Fig. 12. a). When the density of the top stratum is higher (Case Ib), no liquefaction is observed in the soil column (Fig. 12. b). In the case Ic, the initial conditions of the upper $8\ m$ are kept as in case Ib, and lower $12\ m$ of the clean sand column are assumed to be at loose initial states ($e_0 = 0.975$). It is observed that liquefaction occurs throughout almost all the lower stratum after $20s$ of loading (Fig. 12. c). The excess pore pressure in the upper layer increases in comparison with the case Ib. This is mainly induced by the liquefaction of the lower layer.

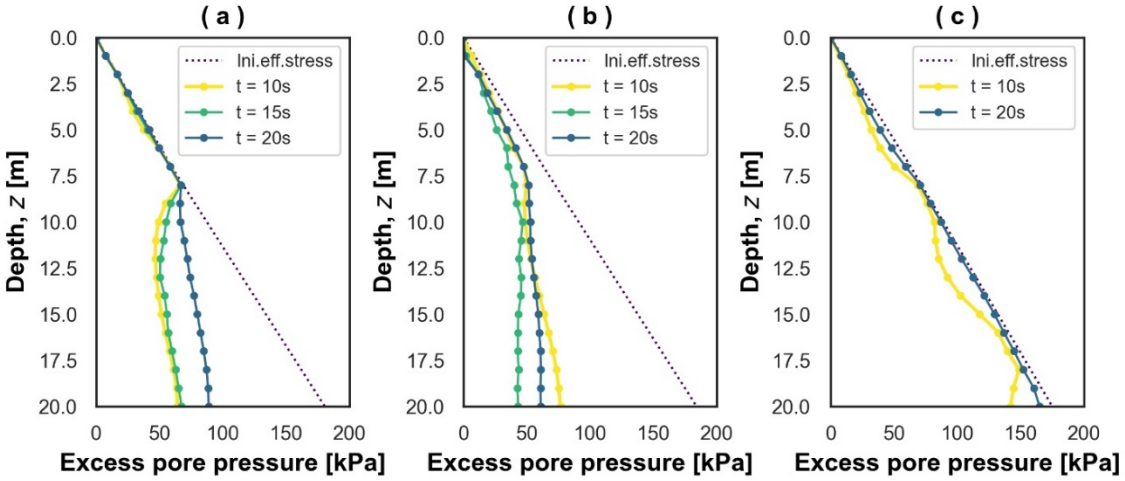

Fig. 12. Results of excess pore pressure soil for different times during seismic loading: a) Case Ia, b) Case Ib, and (c) Case Ic.

The excess pore pressure evolutions over the depth for different initial densities in the upper layer for case II are shown in Fig. 13. It is seen that liquefaction occurs throughout almost all the upper stratum for the void ratio $e = 0.96$ (Case IIa). For the denser state (Case IIb to Case IId), the excess pore pressure remains in the safe region during the shaking. Liquefaction is not observed in the deepest layers during shaking for the four cases analysed. Furthermore, it is possible to observe some dilations on this layer for the denser state (Case IId). The critical state line for silty sand with FC around 40% moves downward in comparison with the silty sand with FC around 17% (Fig. 8)

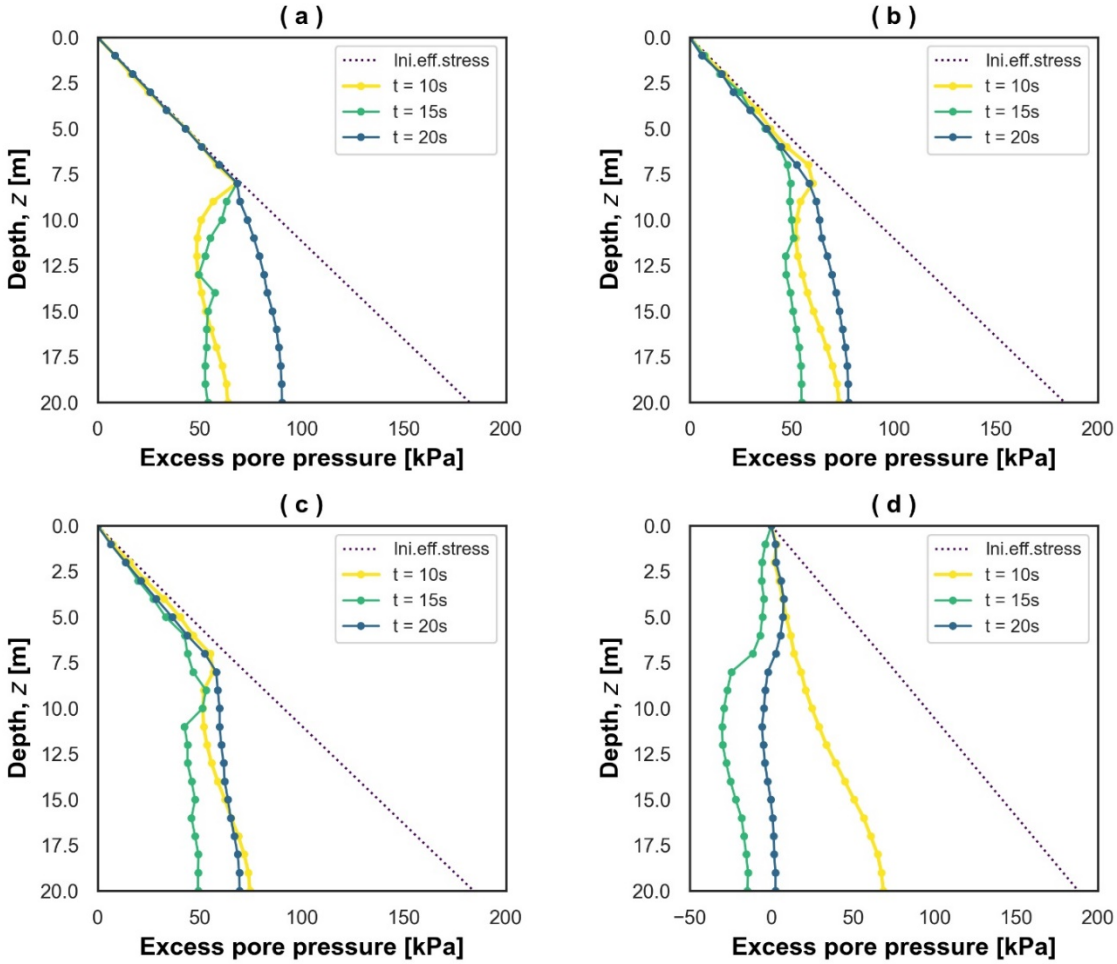

Fig. 13. Results of excess pore pressure soil for different times during seismic loading: a) Case IIa, b) Case IIb, c) Case IIc and d) Case IId

According to the simplified procedures, the increase of the FC does not cause a monotonic increase in liquefaction potential. However, the presented numerical results seem to indicate otherwise. Fig. 14 shows the influence of the FC (5%, 20%, 40% and 65%) in the susceptibility to liquefaction for four void ratios ($e = 0.80, 0.85, 0.90$ and 0.95) in terms of excess pore pressure ratio (r_u) along with depth where r_u is defined as the ratio between the excess pore water pressure and the initial effective stress. The relative position of the critical state lines for different FC (Fig. 14) influences the contractive-dilative behaviour of the clean and silty sand through the state parameter – MPZ constitutive model. It is possible to observe that confining pressure lower than $100\ kPa$ ($(p'/p_a)^{\xi_c} = 1$), similar at the confining pressure

along with the upper layer, and high void ratio (e = 0.95) produces liquefaction only in the first 4 m of upper layer for 20% FC and the first 8m for 40% FC.

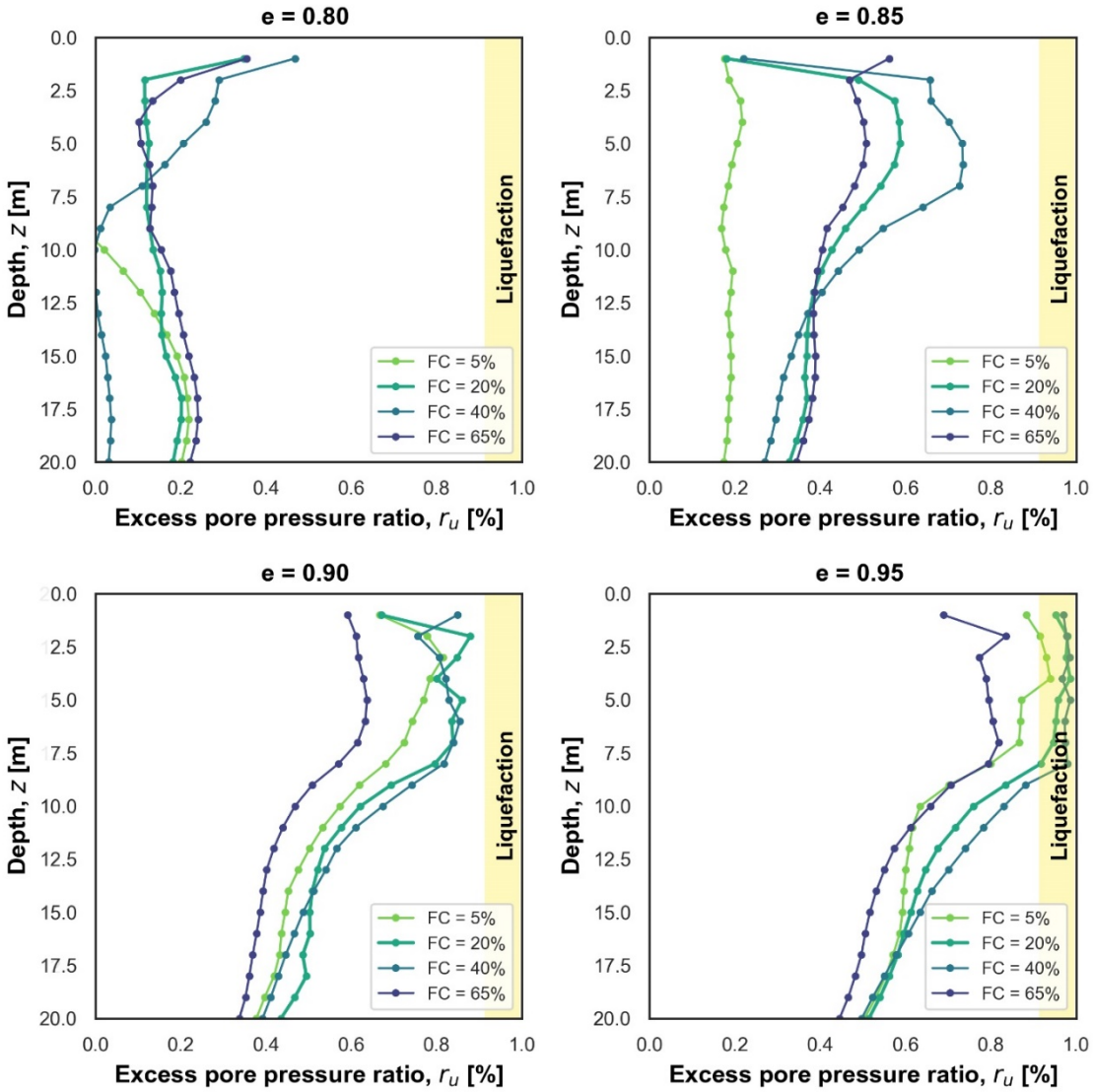

Fig. 14. Results of excess pore pressure ratio along the soil column for different fines content of the upper layer of the silty sand at the end of the earthquake for different initial void ratio e

When the FC of the layer is 65% and the confinement stresses are low, no liquefaction is observed for the voids ratio between 0.8 and 0.95. The same applies to the upper layer with FC lower than 5%. There is an increase in the liquefaction potential between the depths of 2m and 5m. This shows that liquefaction susceptibility is not given only by density or FC as evaluated with simplified methods. The influence of both the confinement pressure and the void ratio, as well as the location of the critical state line, influence and vary the potential liquefaction of the

layer, as shown in Fig. 14. The state parameter plays a fundamental role in the evaluation of the liquefaction potential through constitutive models that adequately reproduce the liquefaction.

These numerical analysis results also corroborate previous findings from the simplified methodologies, which showed that LPI estimations tend to over predict liquefaction manifestations. Compared to the numerical approach, simplified methodologies are fast and straightforward to apply, and they do not require extensive calibrations for their application. Both methods lead to the prediction of liquefaction manifestations at the K1 Site, in agreement with the observations after the Christchurch event. However, the simplified procedures are not able to fully characterise the heterogeneity of the soil column and its behaviour during a seismic event. These approaches are based on regression analysis of liquefaction case histories of soil profiles from different geomorphological settings, most of which involve low FC sites. Instead, Christchurch is characterised by a complex stratigraphy with soil profiles with higher variability of FC. This results in the simplified procedures over-predicting the extent of potentially liquefiable layers due to significant uncertainties in the soil stratigraphy characterisation, FC estimation and, thus, their influence on the identification of potentially liquefiable layers.

5 CONCLUSION

This paper presents a numerical approach for estimating the effect of the FC on liquefaction potential on the Christchurch soils by finite element fully solid-fluid coupled formulation. The constitutive model used combines the versatile and hierarchical formulation of the generalised plasticity theory with the critical state framework and introduces state-dependency for sands and silty sands through the state parameter. Based on previous experimental data on

Christchurch soils, the state parameter is chosen to combine critical state parameters and initial state to estimate the influence of the FC on the liquefaction of different initial soil columns.

The numerical approach shows that higher FC does not prevent liquefaction but rather depends substantially on the initial state of the soil, given by confinement pressure and initial voids ratio. The determination of the critical state line for different FC influences the initial state and the state parameter. Positive initial state parameter shows that the soil columns reach liquefaction. These results demonstrate that liquefaction is likely to occur in the selected location despite the high FC, which agrees with the observations.

Liquefaction across several Christchurch sites is also assessed using 12 simplified procedures based on in-situ penetration testing (6 CPT-based and 6 SPT-based). It is shown that, as these methods do not take into account the effect of contractive-dilative behaviour of sand during shearing, their application to sands with fines can result in over-prediction of liquefaction and unreliable results.

Overall, the simplified approaches result in being valuable methods for skimming the liquefaction potential of large urban areas, as they do not require a vast amount of data for their application. However, numerical simulations must be used to verify empirical estimates in complex geomorphological settings like Christchurch as they provide remarkable insights into the mechanics of soil liquefaction and can more realistically represent the effect of non-plastic fines content on the liquefaction potential of soils during a seismic event.

6 ACKNOWLEDGEMENTS

The first author gratefully acknowledges the financial support for his research visit at University College London granted by the Spanish Ministry of Education under the mobility

program “José Castillejo” (CAS18/00171) and the economic support provided by the Spanish Ministry MINECO under project ALAS (BIA2016-76253-P) and project PLAND (PID2019-105630GB-I00). The authors are also grateful to Myrto Papaspiliou and Crescenzo Petrone from Willis Research Network, Liam Wotherspoon from QuakeCoRE, and UCL CEGE Department, which have supported this research project through the Urban Sustainability and Resilience Doctoral Training School at University College London. We also acknowledge the New Zealand Geotechnical Database (NZGD) and its sponsors, the Ministry of Business, Innovation and Employment and the New Zealand Earthquake Commission (EQC), for providing the geotechnical data used.

7 REFERENCES

Amoroso S, Rollins KM, Andersen P, et al. (2020) Blast-induced liquefaction in silty sands for full-scale testing of ground improvement methods: Insights from a multidisciplinary study. Eng Geol 265:105437. https://doi.org/10.1016/j.enggeo.2019.105437

Ancheta TD, Darragh RB, Stewart JP, et al (2014) NGA-West2 database. Earthq Spectra 30:989–1005

Bandini V, Coop MR (2011) The influence of particle breakage on the location of the critical state line of sands. In: Soils and Foundations. pp 591–600

Beavan J, Fielding E, Motagh M, et al (2011) Fault location and slip distribution of the 22 February 2011 MW 6.2 Christchurch, New Zealand, earthquake from geodetic data. Seismol Res Lett 82:789–799. https://doi.org/10.1785/gssrl.82.6.789

Been K, Jefferies MG (1985) A state parameter for sands. Géotechnique 35:99–112. https://doi.org/10.1680/geot.1985.35.2.99

Bertelli S, Manzanal D, Lopez-Querol S, et al (2019) Numerical simulation of observed liquefaction phenomena from the 2011 Christchurch event. In: SECED 2019. Greenwich, London, pp 1–9

Beyzaei CZ, Bray JD, Cubrinovski M, et al (2018) Laboratory-based characterization of shallow silty soils in southwest Christchurch. Soil Dyn Earthq Eng 110:93–109. https://doi.org/10.1016/j.soildyn.2018.01.046

Biot MA (1941) General theory of three-dimensional consolidation. J Appl Phys 12:155–164.

https://doi.org/10.1063/1.1712886

Boulanger R, Idriss IM (2014a) CPT and SPT Based Liquefaction Triggering Procedures (Report No. UCD/CGM-14/01). CeMemphisEdu 134

Brackley HL (2012) Review of liquefaction hazard information in eastern Canterbury , including Christchurch City and parts of Selwyn , Waimakariri and Hurunui Districts

Brown LJ, Weeber JH (1992) Geology of the Christchurch urban area. Inst Geol Nucl Sci Geol map

Cappellaro C (2019) The Influence of Fines Content , Fabric and Layered Structure on the Undrained Cyclic Behaviour of Christchurch Sandy Soils. University of Canterbury

Cappellaro C, Cubrinovski M, Bray JD, Chiaro G, Riemer MF, Stringer ME (2021) Liquefaction resistance of Christchurch sandy soils from direct simple shear tests. Soil Dyn Earthq Eng 141:106489. https://doi.org/10.1016/j.soildyn.2020.106489

Cavallaro A, Capilleri P, Grasso S (2018): Site Characterization by in Situ and Laboratory Tests for Liquefaction Potential Evaluation during Emilia Romagna Earthquake. Geosciences, Special Issue: "Site-Specific Seismic Hazard Analysis: New Perspectives, Open Issues and Challenges", Geosciences 2018, 8(7), 242, pp. 1 - 15. (ISSN: 2076-3263) DOI:10.3390/geosciences8070242.

Cheng K, Zhang J, Miao Y, Ruan B, Peng T (2019) The effect of plastic fines on the shear modulus and damping ratio of silty sands. B Eng Geol Environ 78:5865-5876. https://dor.org/10.1007/s10064-019-01522-1

Cuomo S, Moscariello MG, Manzanal D, Pastor M, Foresta V (2018) Generalized plasticity constitutive model applied to wetting of unsaturated pyroclastic soil. Computers and Geotechnics. vol. 99 p. 191 – 202. https://doi.org/10.1016/j.compgeo.2018.03.006

Ecemis N, Karaman M (2014) Influence of non-/low plastic fines on cone penetration and liquefaction resistance. Eng Geol 181:48–57. https://doi.org/10.1016/j.enggeo.2014.08.012

Fernandez Merodo JA, Pastor M, Mira P, et al (2004) Modelling of diffuse failure mechanisms of catastrophic landslides. Comput Methods Appl Mech Eng 193:2911–2939. https://doi.org/10.1016/j.cma.2003.09.016

Fontana D, Amoroso S, Minarelli L, Stefani M (2019) Sand Liquefaction Induced By a Blast Test: New Insights On Source Layer and Grain-Size Segregation Mechanisms (Late Quaternary, Emilia, Italy). J Sediment Res 89:13–27. https://doi.org/10.2110/jsr.2019.1

Ghaboussi J, Wilson EL (1973) Flow of compressible fluid in porous elastic media. Int J Numer Methods Eng 5:419–442. https://doi.org/10.1002/nme.1620050311

Goudarzy M, König D, Schanz, T (2016) Small strain stiffness of granular materials containing fines. Soils and Foundations, Volume 56, Issue 5, 2016, Pages 756-764,ISSN 0038-

0806,https://doi.org/10.1016/j.sandf.2016.08.002.

Grasso S, Maugeri M (2008) The Seismic Dilatometer Marchetti Test (SDMT) for Evaluating Liquefaction Potential under Cyclic Loading. In Proc. IV Geotechnical Earthquake Engineering and Soil Dynamic; Sacramento, USA, May 18-22, 2008. Geotechnical Earthquake Engineering and Soil Dynamics IV GSP 181 © 2020 ASCE, Geo Institute, ISBN 978-0-7844-0975-6, 15 p.

Grasso S, Massimino MR, Sammito MSV (2021) New Stress Reduction Factor for Evaluating Soil Liquefaction in the Coastal Area of Catania (Italy). Geosciences 2021, 11, 12. https://doi.org/10.3390/ geosciences11010012

Green RA, Cubrinovski M, Cox B, et al (2014) Select Liquefaction Case Histories from the 2010-2011 canterbury earthquake sequence. Earthq Spectra 30:131–153. https://doi.org/10.1193/030713EQS066M

Hird CC, Hassona FAK (1990) Some factors affecting the liquefaction and flow of saturated sands in laboratory tests. Eng Geol 28:149–170. https://doi.org/10.1016/0013-7952(90)90039-4

Idriss IM, Boulanger RW (2008) Soil Liquefaction during Earthquakes

Idriss IM, Boulanger RW (2004) Semi-empirical Procedures for Evaluating Liquefaction Potential during Earthquakes. In Proceedings of the 11th IC SDEE/3rd ICEGE Proceedings, Berkeley, CA, USA, 7 - 9 January 2004; Volume 1, pp. 32 - 56.

Idriss IM (1999) An Update to the Seed-Idriss Simplified Procedure for Evaluating Liquefaction Potential. In Proceedings of the TRB Workshop on New Approaches to Liquefaction, Washington, DC, USA, 10 January 1999.

Ishihara K (1993) Liquefaction and flow failure during earthquakes. Geotechnique 43:351–451. https://doi.org/10.1680/geot.1993.43.3.351

Iwasaki T, Arakawa T, Tokida K (1984) Simplified Procedures for Assesing Soil Liquefaction During Earthquakes. Soil Dyn Earthq Eng 3:49–58

Iwasaki T, Tatsuoka F, Tokida K, Yasuda S (1978) A practical method for assessing soil liquefaction potential based on case studies at various sites in Japan. In: Proceedings of the 2nd International Conference on Microzonation for Safer Construction-Research and Application, San Francisco, California, USA. pp 885–896

Javanmardi Y, Imam R, Pastor M, Manzanal D (2018) A reference state curve to define the state of soils over a wide range of pressures and densities. Géotechnique Ahead of Print, pp. 1–12. Published online: May 22, 2017. https://doi.org/10.1680/jgeot.16.P.136

Jefferies M, Been K (2016) Soil Liquefaction. A Critical State Approach. Second Edition. CRC Press. 690 Pages. ISBN 9780367873400

Jiang X, Cui P, Ge Y (2015) Effects of fines on the strength characteristics of mixtures. Eng

Geol 198:78–86. https://doi.org/10.1016/j.enggeo.2015.09.011

Juang CH, Ching J, Luo Z, Ku CS (2012) New models for probability of liquefaction using standard penetration tests based on an updated database of case histories. Eng Geol 133–134:85–93. https://doi.org/10.1016/j.enggeo.2012.02.015

Kayabasi A, Gokceoglu C (2018) Liquefaction potential assessment of a region using different techniques (Tepebasi, Eskişehir, Turkey). Eng Geol 246:139–161. https://doi.org/10.1016/j.enggeo.2018.09.029

Lade PV, Ghaboussi J, Inel S, Yamamuro JA (1994) Experimental determination of constitutive behavior of soils. In: International Conference on Association of Computer Methods for Advances in Geomechanics

Li XS (1997) Modeling of dilative shear failure. J Geotech Eng 123:609–616. https://doi.org/10.1061/(ASCE)1090-0241(1997)123:7(609)

Li XS, Dafalias YF (2000) Dilatancy for cohesionless soils. Geotechnique 50, 449–460. https://doi.org/10.1680/geot.2000.50.4.449

López-Querol S, Coop MR (2012) Drained cyclic behaviour of loose dogs bay sand. Geotechnique 62:281–289. https://doi.org/10.1680/geot.8.P.105

López-Querol S, Fernández-Merodo JA, Mira P, Pastor M (2008) Numerical modelling of dynamic consolidation on granular soils. Int J Numer Anal Methods Geomech 32:1431–1457. https://doi.org/10.1002/nag.676

Manzanal D, Fernández Merodo JA, Pastor M (2011a) Generalized plasticity state parameter-based model for saturated and unsaturated soils. Part I: Saturated state. Int J Numer Anal Methods Geomech 35:1347–1362. https://doi.org/10.1002/nag.961

Manzanal D, Pastor M, Merodo JAF (2011b) Generalized plasticity state parameter-based model for saturated and unsaturated soils. Part II: Unsaturated soil modeling. Int J Numer Anal Methods Geomech 35:1899–1917. https://doi.org/10.1002/nag.983

Manzanal D, Pastor M, Merodo JAF, Mira P (2010) A state parameter based generalized plasticity model for unsaturated soils. C - Comput Model Eng Sci 55:293–317. https://doi.org/10.3970/cmes.2010.055.293

Markham CS, Bray JD, Cubrinovski M, Riemer MF (2018) Liquefaction resistance and steady-state characterization of shallow soils within the christchurch central business district. J Geotech Geoenvironmental Eng 144:. https://doi.org/10.1061/(ASCE)GT.1943-5606.0001823

Maurer BW, Green RA, Cubrinovski M, Bradley BA (2015) Fines-content effects on liquefaction hazard evaluation for infrastructure in Christchurch, New Zealand. Soil Dyn Earthq Eng 76:58–68. https://doi.org/10.1016/j.soildyn.2014.10.028

Maurer BW, Green RA, Cubrinovski M, Bradley BA (2014) Evaluation of the liquefaction

potential index for assessing liquefaction hazard in Christchurch, New Zealand. J Geotech Geoenvironmental Eng 140:04014032. https://doi.org/10.1061/(ASCE)GT.1943-5606.0001117

Ministry for Business Innovation & Employment (2018) New Zealand Geotechnical Database (NZGD). https://www.nzgd.org.nz/HelpSupport/AboutNZGD.pdf. Accessed 3 Feb 2020

Monaco P, Marchetti S, Totani G, Calabrese M (2005) Sand liquefiability assessment by Flat Dilatometer Test (DMT). In Proceedings of the XVI ICSMGE, Osaka, Japan, 12–16 September 2005; Volume 4, pp.2693–2697.

New Zealand Geotechnical Database (2013) "Liquefaction and Lateral Spreading Observations", Map Layer CGD0300. https://www.nzgd.org.nz/. Accessed 3 Feb 2020

New Zealand Geotechnical Database (2015) "Conditional PGA for Liquefaction Assessment", Map Layer CGD5110. https://www.nzgd.org.nz/. Accessed 3 Feb 2020

Phan QT, Bui H, Nguyen GD, Bouazza A (2021) Effect of particle rolling resistance on drained and undrained behaviour of silty sand. Acta Geotech. https://doi.org/10.1007/s11440-020-01128-y

Pastor M, Zienkiewicz OC, Chan AHC (1990) Generalized plasticity and the modelling of soil behaviour. Int J Numer Anal Methods Geomech 14:151–190. https://doi.org/10.1002/nag.1610140302

Pitman TD, Robertson PK, Sego DC (1994) Influence of fines on the collapse of loose sands. Can Geotech J 31:728–739. https://doi.org/10.1139/t94-084

Poulos SJ (1981) The steady state of deformation. J Geotech Eng Div ASCE 107:553–562. https://doi.org/10.1016/0148-9062(81)90548-9

Prasomsri J, Takahashi A (2020) The role of fines on internal instability and its impact on undrained mechanical response of gap-graded soils. Soils Found 60:1468-1488. https://doi.org/10.1016/j.sandf.2020.09.008

Qadimi A, Coop MR (2007) The undrained cyclic behaviour of a carbonate sand. Geotechnique 57:739–750. https://doi.org/10.1680/geot.2007.57.9.739

Rahman, M., Dafalias, Y., 2014. Modelling the static liquefaction of sand with low-plasticity fines. Géotechnique 2014 64:11, 881-894

Rahman MM, Lo SR, Gnanendran CT (2008) On equivalent granular void ratio and steady state behaviour of loose sand with fines. Can. Geotech. J. 45, No. 10, 1439–1455, http://dx.doi.org/10.1139/T08-064

Rahman M, Baki M, Lo S (2014) Prediction of undrained monotonic and cyclic liquefaction behavior of sand with fines based on the equivalent granular state parameter. Int. J. Geo-mech. 14, No. 2, 254–266, http://dx.doi.org/10.1061/(ASCE)GM. 1943-5622.0000316.

Rees SD (2010) Effects of fines on the undrained behavior of Christchurch sandy soils.

University of Canterbury

Richart FE, Hall JR, Woods RD (1970) Vibrations of soils and foundations. Prentice-Hall

Robertson PK, Wride CE (1998) Evaluating cyclic liquefaction potential using the cone penetration test. Can Geotech J 35:442–459. https://doi.org/10.1139/t98-017

Sadrekarimi A (2013) Influence of fines content on liquefied strength of silty sands. Soil Dyn Earthq Eng 55:108–119. https://doi.org/10.1016/j.soildyn.2013.09.008

Seed HB, Idriss IM (1971) Simplified procedure for evaluating soil liquefaction potential. ASCE J Soil Mech Found Div 97:1249–1273

Schnaid F (2008) In Situ Testing in Geomechanics: The Main Tests. CRC Press. ISBN: 041543386X

Taylor ML (2015) The geotechnical characterisation of Christchurch sands for advanced soil modelling. University of Canterbury

Thevanayagam S (1998) Effect of Fines and Confining Stress on Undrained Shear Strength of Silty Sands. Journal of Geotechnical and Geoenvironmental Engineering, 124 (6). pp 479-491. doi: 10.1061/(ASCE)1090-0241(1998)124:6(479)

Wotherspoon L, Orense RP, Green R, et al (2014) Analysis of liquefaction characteristics at Christchurch strong motion stations. In: Soil Liquefaction during Recent Large-Scale Earthquakes - Selected Papers from the New Zealand: Japan Workshop on Soil Liquefaction during Recent Large-Scale Earthquakes. pp 33–43

Yang Y, Chen L, Sun R, et al (2017) A depth-consistent SPT-based empirical equation for evaluating sand liquefaction. Eng Geol 221:41–49. https://doi.org/10.1016/j.enggeo.2017.02.032

Yang SL, Sandven R, Grande L (2006) Steady-state lines of sand-silt mixtures. Can. Geotech. J. 43, No. 11, 1213–1219

Youd BTL, Idriss IM, Andrus RD, et al (2001) Liquefaction Resistance of Soils : Summary R Eport From the 1996 Nceer and 1998 Nceer / Nsf Workshops on Evaluation. J Geotech Geoenvironmental Eng 127:817–833. https://doi.org/10.1061/(ASCE)1090-0241(2001)127:10(817)

Youd TL, Idriss IM (2001) Liquefaction Resistance of Soils: Summary Report from the 1996 NCEER and 1998 NCEER/NSF Workshops on Evaluation of Liquefaction Resistance of Soils. J Geotech Geoenvironmental Eng 127:297–313. https://doi.org/10.1061/(ASCE)1090-0241(2001)127:4(297)

Zienkiewicz OC, Chan A, Pastor M, Schrefler B (1999) Computational geomechanics. John Wiley & Sons

Zienkiewicz OC, Chan AHC, Pastor M, et al (1990) Static and dynamic behaviour of soils: a

rational approach to quantitative solutions. I. Fully saturated problems. Proc - R Soc London, A 429:285–309. https://doi.org/10.1098/rspa.1990.0061

Zienkiewicz OC, Chang CT, Bettess P (1980) Drained, undrained, consolidating and dynamic behaviour assumptions in soils. Geotechnique 30:385–395. https://doi.org/10.1680/geot.1980.30.4.385

Zienkiewicz OC, Mroz Z (1984) Generalized plasticity formulation and applications to geomechanics. In: researchgate.net. pp 655–679

Zienkiewicz OC, Shiomi T (1984) Dynamic behaviour of saturated porous media; The generalized Biot formulation and its numerical solution. Int J Numer Anal Methods Geomech 8:71–96. https://doi.org/10.1002/nag.1610080106

Zlatović S, Ishihara K (1995) On the influence of nonplastic fines on residual strength. First Int. Conf. Earthq. Geotech. Eng. 239–244

LIST OF FIGURES

LIST OF TABLES